

## Near-Equilibrium Chemical Force Microscopy

Raymond W. Friddle, Paul Podsiadlo,<sup>†</sup> Alexander B. Artyukhin, and Aleksandr Noy\*

Chemistry, Materials, Energy and Life Sciences Directorate, Lawrence Livermore National Laboratory, Livermore, California 94550

Received: October 1, 2007; In Final Form: December 17, 2007

Molecular force spectroscopy experiments probe the stochastic kinetics of individual intermolecular bond rupture under external loading. While there are numerous examples describing rupture kinetics under fast-loading, far from equilibrium conditions, bond rupture at slow loading rates near equilibrium conditions is seldom explored. We use an analytical and numerical approach to show that rupture forces in this qualitatively different regime reach an equilibrium plateau value that is a function of the probe stiffness and the free energy difference between the bound and dissociated state of the bond. Chemical force microscopy measurements of the interaction between a small number of well-defined COOH functional groups confirm these predictions and show the expected scaling of the force plateau values with the square root of the probe stiffness. Finally, we discuss the implications of these results for the interpretation of force spectroscopy experiments.

### Introduction

Researchers can explore potential energy landscapes of intermolecular interactions by using tiny springs such as atomic force microscope cantilevers, bioforce probes, or optical traps to probe ligand–receptor binding,<sup>1–4</sup> protein unfolding,<sup>5,6</sup> cell adhesion,<sup>7,8</sup> and interactions between basic chemical functional groups.<sup>9</sup> The classic work by Bell<sup>10</sup> established the basic framework for understanding the kinetics of forced bond rupture by recognizing that an external force leads to an exponential amplification of Kramers' rate of escape<sup>11,12</sup> from the bound state. Evans<sup>13</sup> and others<sup>14–16</sup> used Bell's formalism to show that the force required to break an adhesive bond is not unique but instead is a function of the loading rate and the shape of the interaction potential. Therefore, measuring the bond rupture forces over a range of loading rates, an approach termed dynamic force spectroscopy (DFS), provides a way to determine fundamental kinetic parameters of the bond such as the kinetic off-rate and the distance to the transition state.

The vast majority of DFS models focus on predicting rupture when the system is driven far from equilibrium, where the rupture process is irreversible. Most of these works assume that forced rupture in the near-equilibrium regime, where the loading rates are sufficiently slow to enable rebinding, is inaccessible experimentally and thus is unimportant. Consequently, even as the effects of rebinding at slow loading rates have been addressed theoretically,<sup>17</sup> experimentalists have largely ignored this regime. We demonstrate that the near equilibrium rupture regime is accessible in force spectroscopy experiments in which the interacting molecules are rigidly linked to the surface of the force probe, and that unbinding kinetics in this regime is qualitatively different from the behavior observed in far from equilibrium DFS measurements. We consider the transition between bound and unbound states at slow loading rates and show that the measured rupture forces approach a rupture force

plateau value that is a simple function of the force probe stiffness and the free energy difference between the bound and unbound states.

### Methods

**Materials and Chemicals.** To obtain a large range of cantilever spring constants, we used a set of commercially available AFM probes: (1) The Olympus Bio-Lever B with  $k = 0.006$  N/m; (2) The Veeco MicroLevers (Santa Barbara, CA) with  $k = 0.01, 0.02, 0.03, 0.05, 0.1,$  and  $0.5$  N/m; and (3) NanoWorld PointProbe (Neuchatel, Switzerland) with  $k = 2.8$  N/m. (These values are the nominal spring constant values and are quoted here only to identify the cantilevers; the actual values for the spring constants used for our measurements were calibrated as described in the next section.)

AFM probes and polished (100) silicon wafers were used as received. Ethanol and 16-mercaptohexadecanoic acid were purchased from Aldrich and used as received. To modify the surfaces with well-defined chemical functionalities, we first cleaned the tips and silicon pieces in piranha solution (3:1 mixture of concentrated sulfuric acid and hydrogen peroxide, highly corrosive!). Subsequently we have coated the probes and wafers with 50 Å of chromium followed by 1000 Å of gold. The coatings were deposited by thermal evaporation at a rate of  $\sim 1$  Å/s. We then immersed the AFM probes and substrates in freshly made 5 mM solutions of mercaptohexadecanoic acid in ethanol for 12 h (overnight). The probes and samples were taken out of solution immediately before the experiment. Prior to mounting in the microscope, probes and samples were rinsed with ethanol and dried under a filtered nitrogen stream.

**Cantilever Calibration and Dynamic Force Spectroscopy.** We have used an MFP-3D atomic force microscope (Asylum Research, Santa Barbara, CA) for our measurements. All measurements were carried out in an EtOH meniscus formed between the silicon wafer and AFM tip holder to ensure complete immersion of the tip for the duration of the experiments. Large variations in the spring constants of the commercial cantilevers, as well as the effects of the deposition of Cr/Au

\* Corresponding author. E-mail: noy1@llnl.gov.

<sup>†</sup> Permanent address: Chemical Engineering Department, University of Michigan, Ann Arbor, Michigan.

layers, require individual calibration of every cantilever. We calibrated our cantilevers individually using the thermal resonance method and MFP-3D built-in procedures immediately prior to use.<sup>18</sup> Deposition of the Cr/Au layers resulted in a significant increase of the spring constants for all of the cantilevers with values below 0.5 N/m.

**Adhesion Force Measurements and Data Processing.** We measured the adhesion forces by recording AFM cantilever deflection in the “force curve” cycle. The magnitude of the pull-off jump in the retraction part of the curve provided the measure of the adhesion force. To measure binding force as a function of loading rate, we used a feature of the instrument that allowed for delaying retraction after the tip has made contact with the substrate, which also ensured equilibration of the system.

A predetermined set of velocities was chosen based on the spring constant value for each cantilever. To quantify these uncertainties in the measurement and obtain significant statistics to determine the binding force distributions, we recorded at least 100 individual binding forces for low velocities and as high as 300 forces for high velocities for every loading rate value. To avoid introducing systematic error in the data associated with tip wear, we varied the loading rates in random order. IgorPro data analysis software (WaveMetrics, Lake Oswego, OR) and a set of custom-written analysis procedures was used to extract the values of the adhesion force from the force curves collected by the instrument.

**Numerical Simulations.** All numerical simulations utilized custom-written code in IgorPro data analysis software (WaveMetrics, Lake Oswego, OR). For all simulation runs, we assumed that the bond potential could be represented by a Morse potential  $U(x) = U_0[1 - \exp(-2b(x/x_0 - 1))]^2 - U_0$  with  $U_0 = 10 k_B T$ ,  $x_0 = 1 \text{ \AA}$ , and  $b = 1$ .

## Results and Discussion

**Analytical Model.** We begin by considering a simple model of loading an intermolecular potential  $U(x)$  with a harmonic spring  $V(x,t) = 1/2k(x - vt)^2$ , where  $x$  is the direction of applied force,  $k$  is the spring stiffness, and  $v$  is the pulling speed. For simplicity, both the bound state of  $U(x)$  and the initial minimum of  $V(x,t = 0)$  are located at  $x = 0$ . The combined energy landscape  $E(x,t) = U(x) + V(x,t)$  then ensures that at time  $t = 0$  (and at zero-applied force) there is an impenetrable barrier to bond rupture. Thus, if the interacting molecules are rigidly connected to a harmonic force probe, then the lifetime of the bound state remains essentially infinite until the probe potential is translated far enough to create a second metastable state (Figure 1 and Figure 2A). Qualitatively, a harmonic force probe potential ensures that a bond can rupture only if the applied force exceeds a certain minimum value. Note that this constraint is fundamentally different from a typical DFS model that assumes that any noncovalent bond will spontaneously dissociate if left at zero force for a sufficient amount of time.<sup>13</sup> That model in effect describes loading with a semiharmonic probe potential (see Figure 2B) and is mostly applicable for describing experiments where molecules are connected to a force probe by flexible tethers.<sup>19</sup> Note that the differences between these two kinetics becomes experimentally significant only in the near-equilibrium regime<sup>17</sup> when the bond is loaded slow enough for the rebinding process to be significant.<sup>20</sup> When the loading rates are fast, the applied force exceeds this minimum value required for bond dissociation very quickly, rebinding is negligible, and the behavior of both systems becomes virtually identical.

To calculate the rupture force in the near-equilibrium regime, we assume the pulling process to be quasi-static, such that the

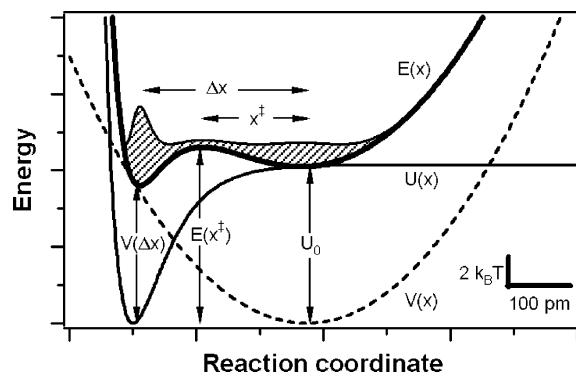


**Figure 1.** Schematic of a potential energy landscape  $E(x)$  (bold line) representing the loading of an intermolecular bond approximated by a Morse potential  $U(x)$  (thin line; see Methods for the parameter values) by a harmonic force probe  $V(x)$  (dotted line).  $\Delta x$ ,  $x_{\ddagger}^{\ddagger}$  represent the locations of the bound state and transition state relative to the probe minimum. Hatched area is the superimposed equilibrium distribution of states. The secondary minimum created by the loading potential represents the unbound state.

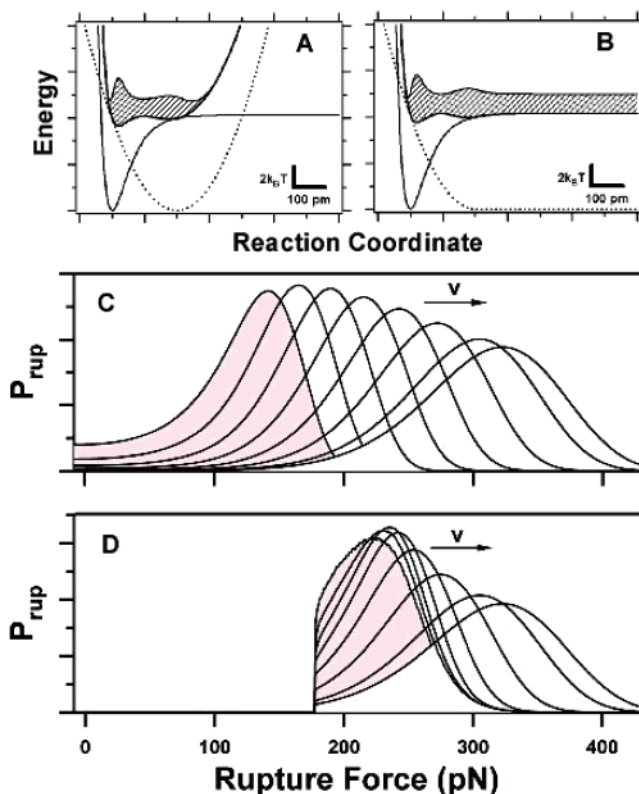


**Figure 2.** (A,B) A comparison of the calculated potential energy landscapes representing loading of the Morse potential with a harmonic probe (panel A) and a semiharmonic probe (panel B). (C,D) Rupture force distributions calculated numerically from eq 6 for loading by a semiharmonic (panel C) and harmonic (panel D) probe over an identical set of pulling velocities ranging from 8 nm/s (purple) to 621 nm/s (blue). The probe stiffness,  $k$ , was 0.8 N/m in both cases.

equilibrium Boltzmann distribution approximates the distribution of states over the potential energy surface at every instance. Once the pulling potential creates a second metastable state, the difference in the average internal energy between the bound and unbound states decreases according to (Figure 1)

$$\Delta\langle U \rangle = U_0 - V(0, vt = \Delta x) = U_0 - \frac{f^2}{2k} \quad (1)$$

where  $U_0$  is the internal energy of the intermolecular bond,  $f = kv$  is the applied force, and  $\Delta x = f/k$  is the average distance between the bound and unbound state minima. Under the quasi-static assumption, the average rupture transition must occur at a position where the total free energy change is zero,  $\Delta\langle U \rangle - T\Delta S = 0$ . Applying this condition to eq 1, we find

$$f_{\text{eq}} = \sqrt{2k(U_0 - T\Delta S)} = \sqrt{2k\Delta G} \quad (2)$$

where  $\Delta G$  is the equilibrium free energy change between the bound and the unbound state. Equation 2 provides a number of significant insights. Perhaps the most important conclusion is that even in the near-equilibrium regime the unbinding force is not unique for any given bond; instead it is proportional to the square root of the stiffness of the probe,  $k$ . The same dependence on probe stiffness was predicted by Evans<sup>17</sup> using a kinetic approach. Significantly, this relationship provides a straightforward way to estimate the free energy difference between the bound and unbound states, by measuring the rupture forces at different probe stiffness values. Note also that if the probe stiffness is very large, eq 2 would break down as the combined energy landscape would no longer have two energy minima and would not permit a transition between the bound and unbound state; this regime of force spectroscopy is ideally suited for direct interaction potential reconstruction approaches.<sup>21–23</sup>

Further analysis of eq 2 reveals the important role that the entropy difference between the bound and unbound states plays in determining the value of the near-equilibrium rupture force. Intuitively, the entropy change  $\Delta S$  measures the differences in the spatial spread of the bound and unbound states at the moment of unbinding. If we approximate these two states as harmonic oscillators with curvatures  $k_i = m\omega_i^2$ , where  $\omega_i$  is the natural angular frequency of state  $i$  and  $m$  is the inertial mass, then the entropy is approximately,  $S_i \approx k_B[\ln(k_B T/\hbar\omega_i) + 1]$ . The entropy change between the bound and unbound states is then  $\Delta S = k_B T \ln(\omega_b/\omega_u)$ , and the equilibrium unbinding force takes the form

$$f_{\text{eq}} = \sqrt{2k[U_0 - k_B T \ln(\omega_b/\omega_u)]} \quad (3)$$

We can also analyze this system using Kramers' approximation of Smoluchowski transport in a strongly damped system.<sup>12</sup> For diffusive crossings that require many attempts, the unbinding and rebinding rates are

$$k_+(t) = \frac{\omega_b \omega_{\ddagger}}{2\pi\gamma} \exp\left[-\frac{\Delta E(t)_{b\ddagger}}{k_B T}\right] \quad (4)$$

$$k_-(t) = \frac{\omega_u \omega_{\ddagger}}{2\pi\gamma} \exp\left[-\frac{\Delta E(t)_{u\ddagger}}{k_B T}\right] \quad (5)$$

respectively, where  $\gamma$  is the damping coefficient of the system. Here,  $\Delta E(t)_{b\ddagger} = E(x_{\ddagger}^{\ddagger}) - f^2/2k$  and  $\Delta E(t)_{u\ddagger} = E(x_{\ddagger}^{\ddagger}) - U_0$ . At equilibrium, the unbinding and rebinding transition rates are equal,  $k_+(t) = k_-(t)$ , which produces a solution identical to eq 3.

Both approaches illustrate the link between the value of the rupture force, the stiffness of the probe, and the curvatures of the energy surface  $\omega_b$  and  $\omega_u$ . If we want to use eq 3 to estimate the potential depth  $U_0$ , then we need to consider the relative stiffness of the bound and unbound states. If the probe is soft, as is the case for most biological force spectroscopy experiments, the measured force would underestimate  $U_0$ . Equations 2 and 3 also explain the fundamental difference between loading

bonds with a semiharmonic and harmonic force probes (Figure 2A,B). A semiharmonic probe permits large entropic freedom in the unbound state, in which case the change in entropy upon unbinding overcomes the intrinsic energy of the bond and permits spontaneous dissociation at zero-applied force, in accordance with the prediction of most DFS models.<sup>17</sup>

**Numerical Simulations.** To describe the rupture process over the full range of loading rates, we turn to numerical simulations. Here, we cannot assume that the rebinding rate is negligible and instead must use the complete master equation

$$\partial_t P_b(t) = -P_b(t)k_+(t) + P_u(t)k_-(t) \quad (6)$$

where  $P_b(t)$  and  $P_u(t)$  are the probabilities of finding a particle in the bound and unbound states, respectively, and  $k_+(t)$  and  $k_-(t)$  are the time-dependent unbinding and rebinding kinetic rates. Following Kramers' approach,<sup>12</sup> we calculate the transition rate as

$$k_+(t)^{-1} = \frac{\gamma}{k_B T} \int_{\Omega_b} e^{-E(x,t)/k_B T} dx \int_{\Omega_{\ddagger}} e^{-E(x,t)/k_B T} dx \quad (7)$$

where  $\Omega_b$  and  $\Omega_{\ddagger}$  designate integration over the bound and transition states, respectively. A similar relationship is used to calculate the rebinding rate  $k_-(t)$ . Numerical solution of eq 6 is straightforward given that  $P_b + P_u = 1$ . Calculated rupture force distributions when loading with a harmonic potential (Figure 2D) clearly show the "forbidden" region in the rupture force distribution where no rupture events occur regardless of how slow the loading rate is. In contrast, rupture force distributions obtained using a semiharmonic potential (Figure 2C) show the classic DFS behavior in which unbinding events could occur at all values of the applied force. As the pulling velocity increases, the distributions for both types of probe potentials converge.

The force spectra calculated for harmonic potential loading (Figure 3A) show two distinct regions. At slow loading rates, the rupture force values approach a plateau where the force becomes independent of the loading rate. At high pulling velocities, the rupture spectrum transitions into a loading rate-dependent regime that scales best with  $f \sim (\ln kv)^{1/2}$ , as predicted for a one-dimensional cusplike potential.<sup>16,24</sup> This graph is also qualitatively similar to the force spectra calculated by Evans for transition from near-equilibrium to far-from equilibrium regimes.<sup>17</sup> As predicted by eq 2, the plateau force scales well with the square root of the probe stiffness (Figure 3A, inset). A fit of eq 2 to these data yields an average free energy change of  $\Delta G = 8.21 k_B T$ . Note that this value underestimates the value of the potential depth ( $U_0 = 10 k_B T$ ) used in the simulation in accordance with our prediction that the measured free energy change would underestimate  $U_0$  for loading with a soft spring. Moreover, this value compares quite favorably with the average of the exact free energy change,  $\Delta G = -k_B T \ln(Z_u/Z_b) = 8.17 k_B T$  for these probe stiffnesses when calculated using the configurational integrals of the bound ( $Z_b$ ) and unbound ( $Z_u$ ) states given by

$$Z_i = \int e^{-U_i(x)/k_B T} dx \quad (8)$$

### Chemical Force Microscopy in Near-Equilibrium Regime.

The most important result that we report here is the experimental observation of the predicted force plateau scaling in a series of measurements using AFM tips with different spring constants  $k$ . To control the interaction between the tip and surface, we have functionalized both the AFM tips and the sample surfaces with well-defined self-assembled monolayers of 16-mercapto-

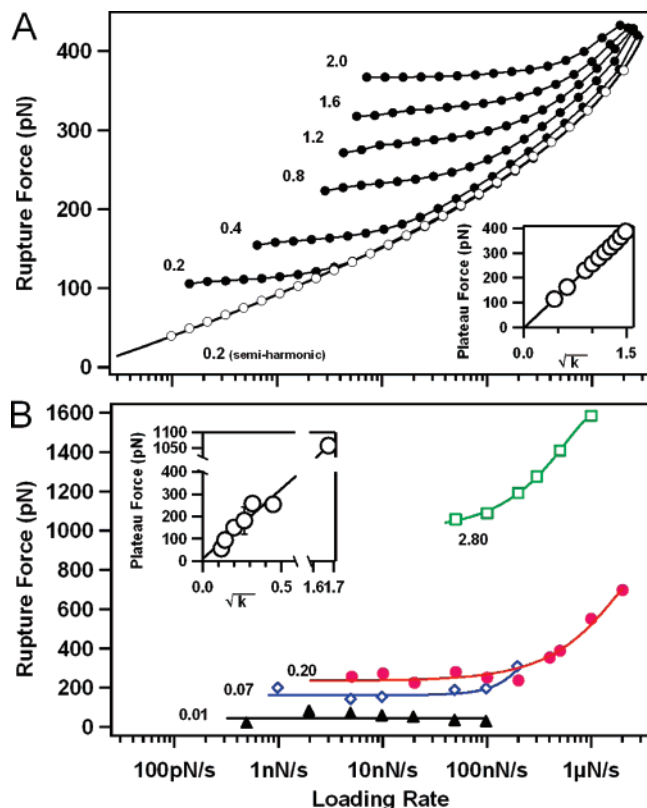


**Figure 3.** Comparison of measured and calculated force spectra for loading with harmonic probes of different stiffness (numerical labels indicate the spring constant of the probe,  $k$ , in units of N/m.) (A) Rupture force values (filled circles) calculated as numerical solution of eq 6. Open circles represent the solution of the same equation for a semi-harmonic force probe where the rebinding was negligible ( $k_{-}(t) \approx 0$ ). The bold line passing through the open circle points is a fit of the analytical relationship  $f = 2a\{1 - [b + c \ln(1/kv)]^{1/2}\}$ , as described by Dudko et al.<sup>24</sup> (B) Interaction forces between AFM cantilevers of different spring constants and sample surfaces functionalized with COOH functional groups (not all spectra are shown for clarity, and solid curves act as guide to the eye). Insets: calculated (panel A) and measured (panel B) plateau forces as a function of the square root of the spring constant.

hexadecanoic acid terminating in COOH groups. Binding forces measured between these tips and surfaces in ethanol (Figure 3B) show all the features predicted in the simulations: the measured rupture forces plateau at low loading rates and transition to a loading rate-dependent regime at higher pulling speeds. Significantly, the experimental results show the predicted  $\sqrt{k}$  scaling of the plateau forces (Figure 3B, inset). The slope of this dependence produces a free energy value of  $\Delta G = 47.21 \pm 0.06 k_B T$ . Because the forces measured in these experiments encompassed interactions of multiple individual functional groups, we use continuum contact mechanics estimates based on the Johnson, Kendall, and Roberts (JKR) model to obtain an estimate of the average number of interacting functional groups.<sup>25,26</sup> Previous estimates showed that in this configuration the tip-sample interaction comprises approximately  $20 \pm 10$  functional groups.<sup>9,27</sup> Therefore, if we assume that the interaction represents the hydrogen bonding of COOH groups in ethanol, we estimate the free energy for rupture of a bond between two COOH groups as  $\Delta G_{\text{H-bond}} = 2.3 k_B T$  (5.7 kJ/mol). Although this value compares well with recent thermodynamic estimates<sup>28</sup> of the free energy of a hydrogen bond in ethanol ( $2.1 k_B T$  (5.4 kJ/mol)), we note that it is based on a crude estimate of the contact area and thus needs to be considered as an order of magnitude assessment rather than a precise measurement. It is

also important to consider that the free energy determined here is not referenced to a standard solution state condition. While bridging thermodynamic information determined from force spectroscopy with ensemble experiments in solution is an important goal, it remains outside the scope of the present work.

Finally, we want to comment that the dynamic force spectra measured in molecular systems often show a transition between regions of lower to higher slope. Typically researchers interpret this bend in the force spectrum to represent two barriers on the intermolecular potential energy surface. Our results show that such trends at low loading rates may instead reflect the confinement by the harmonic probe and a transition to near-equilibrium unbinding. For example, a previous work by our group<sup>29</sup> has almost certainly incorrectly attributed a plateau in the dynamic force spectrum to the existence of an outer solvation barrier in the interaction potential. In the future, researchers may distinguish between these effects by measuring the dynamic force spectrum in this region using probes with two different spring constants: if the low-sloping region is caused by an additional barrier in the intermolecular potential, the plateau will not show the characteristic dependence on the square root of the spring constant predicted by eq 2.

We have demonstrated that force spectroscopy measurements conducted at sufficiently slow loading rates can proceed in a near-equilibrium regime that is qualitatively different from the generally accepted DFS models. In this regime, the measured rupture force is independent of the loading rate and instead is proportional to the square root of the loading spring stiffness. This behavior is a direct consequence of the shape of the potential energy landscape defined by the combination of the intermolecular bond potential and the harmonic potential of the loading spring. Chemical force microscopy experiments confirm this behavior and show that it obeys the scaling predicted by the analytical model and numerical simulations. Moreover, we show that measurements of rupture forces in this regime can provide an assessment of the free energy change during bond rupture. This simple technique is applicable to a wide variety of systems and may serve as a routine technique for extracting thermodynamic parameters of bimolecular interactions.

**Acknowledgment.** R.W.F. and A.B.A. acknowledge LLNL Student Employee Graduate Research Fellowships, and P.P. acknowledges funding from the Hertz Fellowship. A.N. acknowledges support from Office of Basic Energy Science (BES), Division of Materials Science and Engineering. We thank Dr. P. Williams for a stimulating discussion in 2003 that alerted us to the importance of rebinding in force spectroscopy experiments. This work was performed under the auspices of the U.S. Department of Energy by Lawrence Livermore National Laboratory under Contract DE-AC52-07NA27344.

## References and Notes

- (1) Merkel, R.; Nassoy, P.; Leung, A.; Ritchie, K.; Evans, E. *Nature* **1999**, *397*, 50.
- (2) Simson, D. A.; Strigl, M.; Hohenadl, M.; Merkel, R. *Phys. Rev. Lett.* **1999**, *83*, 652.
- (3) Evans, E.; Leung, A.; Hammer, D.; Simon, S. *Proc. Natl. Acad. Sci. U.S.A.* **2001**, *61324998*.
- (4) Sulchek, T. A.; Friddle, R. W.; Langry, K.; Lau, E. Y.; Albrecht, H.; Ratto, T. V.; DeNardo, S. J.; Colvin, M. E.; Noy, A. *Proc. Natl. Acad. Sci. U.S.A.* **2005**, *102*, 16638.
- (5) Fernandez, J. M.; Li, H. B. *Science* **2004**, *303*, 1674.
- (6) Schlierf, M.; Li, H.; Fernandez, J. M. *Proc. Natl. Acad. Sci. U.S.A.* **2004**, *101*, 7299.
- (7) Prechtel, K.; Bausch, A.; Marchi-Artzner, V.; Kantlehner, M.; Kessler, H.; Merkel, R. *Phys. Rev. Lett.* **2002**, *89*, 28101.
- (8) Tsang, P. H.; Li, G.; Brun, Y. V.; Freund, L. B.; Tang, J. X. *Proc. Natl. Acad. Sci. U.S.A.* **2006**, *103*, 5764.

- (9) Noy, A.; Vezenov, D.; Lieber, C. *Ann. Rev. Mat. Sci.* **1997**, *27*, 381.
- (10) Bell, G. I. *Science* **1978**, *200*, 618.
- (11) Hanggi, P.; Talkner, P.; Borkovec, M. *Rev. Mod. Phys.* **1990**, *62*, 251.
- (12) Kramers, H. A. *Physica* **1940**, *7*, 284.
- (13) Evans, E.; Ritchie, K. *Biophys. J.* **1997**, *72*, 1541.
- (14) Izrailev, S.; Stepaniants, S.; Balsera, M.; Oono, Y.; Schulten, K. *Biophys. J.* **1997**, *72*, 1568.
- (15) Dudko, O. K.; Filippov, A. E.; Klafter, J.; Urbakh, M. *Proc. Natl. Acad. Sci. U.S.A.* **2003**, *100*, 11378.
- (16) Hummer, G.; Szabo, A. *Biophys. J.* **2003**, *85*, 5.
- (17) Evans, E. *Ann. Rev. Biophys. Biomol. Struct.* **2001**, *30*, 105.
- (18) Hutter, J. L.; Bechhoefer, J. *Rev. Sci. Instr.* **1993**, *64*, 1868.
- (19) Evans, E.; Williams, P. Dynamic Force Spectroscopy: I. Single Bonds. In *Physics of Bio-Molecules and Cells*; Flyvbjerg, H., Jülicher, F., Ormos, P., David, F., Eds.; Springer and EDP Sciences: Heidelberg, Germany, 2002; Vol. 75; pp 147.
- (20) See refs 17 and 19 for the expression defining the threshold loading rate for the cross-over from near-equilibrium to far-from equilibrium regime.
- (21) Cleveland, J. P.; Schaffer, T. E.; Hansma, P. K. *Phys. Rev. B.* **1995**, *52*, R8692.
- (22) Ashby, P. D.; Chen, L. W.; Lieber, C. M. *J. Am. Chem. Soc.* **2000**, *122*, 9467.
- (23) Ashby, P. D.; Lieber, C. M. *J. Am. Chem. Soc.* **2004**, *126*, 16973.
- (24) Dudko, O. K.; Hummer, G.; Szabo, A. *Phys. Rev. Lett.* **2006**, *96*, 108101.
- (25) Johnson, K. L.; Kendall, K.; Roberts, A. D. *Proc. R. Soc. London, Ser. A* **1971**, *324*, 301.
- (26) Luan, B.; Robbins, M. O. *Nature* **2005**, *435*, 929.
- (27) Noy, A.; Frisbie, C. D.; Rozsnyai, L. F.; Wrighton, M. S.; Lieber, C. M. *J. Am. Chem. Soc.* **1995**, *117*, 7943.
- (28) van der Spoel, D.; van Maaren, P. J.; Larsson, P.; Timneanu, N. *J. Phys. Chem. B* **2006**, *110*, 4393.
- (29) Zepeda, S.; Yeh, Y.; Noy, A. *Langmuir* **2003**, *19*, 1457.